



**Providing Choice & Value**  
Generic CT and MRI Contrast Agents

**FRESENIUS  
KABI**

**CONTACT REP**

**AJNR**





**Glutaric Aciduria Type 1: Comparison  
between Diffusional Kurtosis Imaging and  
Conventional MR Imaging**

B. Bian, Z. Liu, D. Feng, W. Li, L. Wang, Y. Li and D. Li

*AJNR Am J Neuroradiol* published online 20 July 2023  
<http://www.ajnr.org/content/early/2023/07/20/ajnr.A7928>

This information is current as  
of July 30, 2025.

# Glutaric Aciduria Type 1: Comparison between Diffusional Kurtosis Imaging and Conventional MR Imaging

 B. Bian, Z. Liu,  D. Feng, W. Li, L. Wang,  Y. Li, and  D. Li



## ABSTRACT

**BACKGROUND AND PURPOSE:** Routine MR imaging has limited use in evaluating the severity of glutaric aciduria type 1. To better understand the mechanisms of brain injury in glutaric aciduria type 1, we explored the value of diffusional kurtosis imaging in detecting microstructural injury of the gray and white matter.

**MATERIALS AND METHODS:** This study included 17 patients with glutaric aciduria type 1 and 17 healthy controls who underwent conventional MR imaging and diffusional kurtosis imaging. The diffusional kurtosis imaging metrics of the gray and white matter were measured. Then, the MR imaging scores and diffusional kurtosis imaging metrics of all ROIs were further correlated with the morbidity scores and Barry-Albright dystonia scores.

**RESULTS:** The MR imaging scores showed no significant relation to the morbidity and Barry-Albright dystonia scores. Compared with healthy controls, patients with glutaric aciduria type 1 showed higher kurtosis values in the basal ganglia, corona radiata, centrum semiovale, and temporal lobe ( $P < .05$ ). The DTI metrics of the basal ganglia were higher than those of healthy controls ( $P < .05$ ). The fractional anisotropy value of the temporal lobe and the mean diffusivity values of basal ganglia in glutaric aciduria type 1 were lower than those in the control group ( $P < .05$ ). The diffusional kurtosis imaging metrics of the temporal lobe and basal ganglia were significantly correlated with the Barry-Albright dystonia scores. The mean kurtosis values of the anterior and posterior putamen and Barry-Albright dystonia scores were most relevant ( $r = 0.721, 0.730$ , respectively). The mean kurtosis values of the basal ganglia had the best diagnostic efficiency with area under the curve values of 0.837 for the temporal lobe, and the mean diffusivity values of the basal ganglia in glutaric aciduria type 1 were lower than those in the control group ( $P < .05$ ). The diffusional kurtosis imaging metrics of the temporal lobe and basal ganglia were significantly correlated with the Barry-Albright dystonia scores. The mean kurtosis values of the anterior and posterior putamen and Barry-Albright dystonia scores were most relevant ( $r = 0.721, 0.730$ , respectively). The mean kurtosis values of the basal ganglia had the best diagnostic efficiency with area under the curve values of 0.837.

**CONCLUSIONS:** Diffusional kurtosis imaging provides more comprehensive quantitative information regarding the gray and white matter micropathologic damage in glutaric aciduria type 1 than routine MR imaging scores.

**ABBREVIATIONS:** AD = axial diffusivity; AK = axial kurtosis; AP = anterior putamen; AUC = under the curve; BAD = Barry-Albright dystonia; CBH = cerebellar hemisphere; CH = caudate head; CR = corona radiata; CS = centrum semiovale; DKI = diffusional kurtosis imaging; DN = bilateral dentate nucleus; FA = fractional anisotropy; FL = frontal lobes; GA-1 = glutaric aciduria type 1; GCDH = glutaryl-CoA dehydrogenase; GP = globus pallidus; HC = healthy control; MD = mean diffusivity; MK = mean kurtosis; P = pons; PL = parietal lobes; PP = posterior putamen; RD = radial diffusivity; RK = radial kurtosis; ROC = receiver operating characteristic curve; SN = substantia nigra; Th = thalamus; TL = temporal lobes

Glutaric aciduria type-1 (GA-1) is a rare autosomal recessive disorder characterized by a deficiency of glutaryl-CoA dehydrogenase (GCDH) activity, often involving the CNS.<sup>1-3</sup> Mutations


in the *GCDH* gene encoding the mitochondrial matrix protein GCDH have been found. They result in defective or missing GCDH and lead to abnormal accumulation of organic acids, such as glutaric acid, 3-hydroxy-glutaric acid, and glutarylcarnitine in the blood,

Received March 21, 2023; accepted after revision June 7.

From the Departments of Radiology (B.B., Z.L., D.L.), and Outpatient Pediatrics (D.F.), and Gene Therapy Laboratory (Y.L.), The First Hospital of Jilin University, Changchun, Jilin, China; and State Key Laboratory of Stem Cell and Reproductive Biology (W.L., L.W.), Chinese Academy of Sciences and University, Beijing, China.

This work was supported by the Natural Science Foundation of Jilin Province, YDZJ202101ZYT5019, YDZJ202101ZYT5084 and National Key Research and Development Program, 2019YFA0110800.

Please address correspondence to Dan Li, MD, Department of Radiology, The First Hospital of Jilin University, Changchun, Jilin, China; e-mail: li\_d@jlu.edu.cn

 Indicates open access to non-subscribers at [www.ajnr.org](http://www.ajnr.org)

 Indicates article with online supplemental data.

<http://dx.doi.org/10.3174/ajnr.A7928>

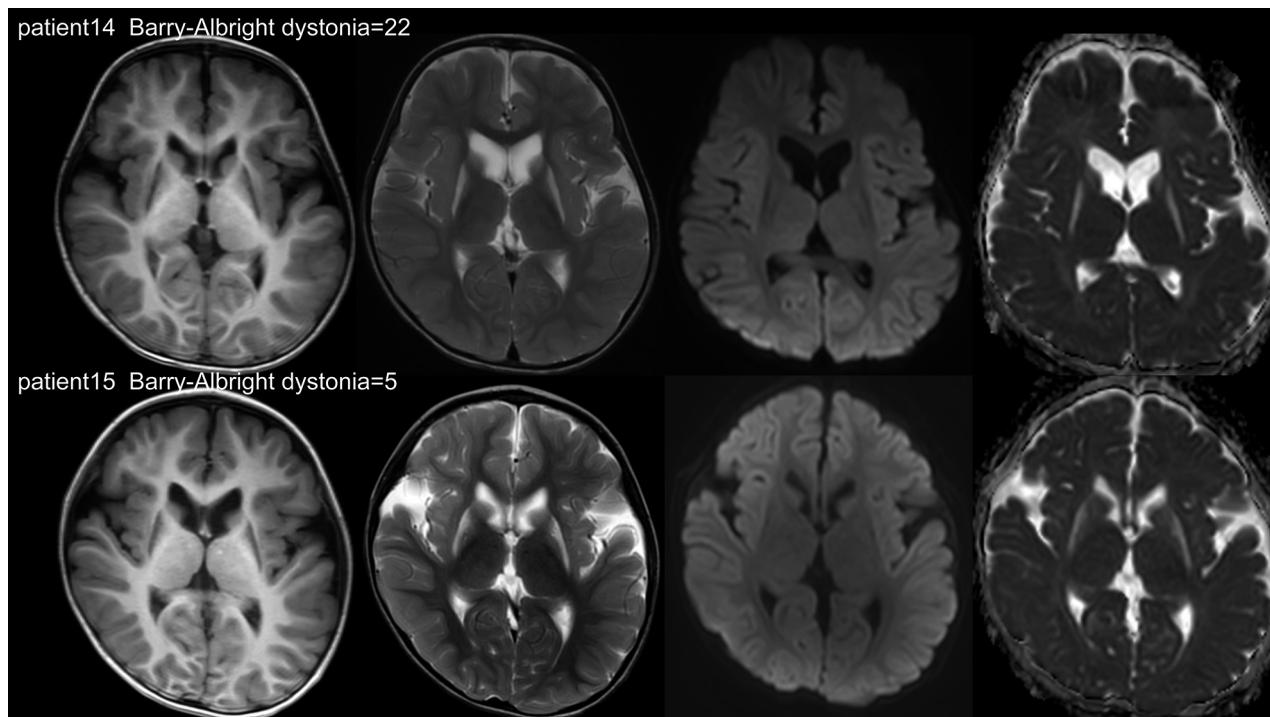


**FIG 1.** Clinoradiologic contradiction. Both patients showed T2WI prolongation and no diffusion restriction in the putamen, but the BAD scores were very different.

urine, CSF, and brain tissue. Bilateral striatal necrosis was previously pathologically and clinically found in patients with GA-1, resulting in a severe dystonic movement disorder.<sup>4-6</sup> The clinical manifestations of patients with GA-1 include an acute encephalopathic crisis precipitated by intercurrent febrile illness, macrocephalus, hypotonia, and choreoathetosis and seizures, and patients usually end with permanent motor and mental disability.

MR imaging findings are an important tool for the diagnosis of GA-1, which include characteristic cyst-like bilateral enlargement of the Sylvian fissures, signal abnormalities, and atrophy of the supratentorial WM and the deep GM structures.<sup>7-9</sup> However, we found a clinoradiologic contradiction in conventional brain MR imaging results. Specifically, we established that patients with GA-1 may have outcomes of dystonia deterioration that are quite different, even if similar abnormal signals of the striatum have been obtained (Fig 1). In addition, Mohammad et al,<sup>8</sup> Sadek et al,<sup>9</sup> and Garbade et al<sup>10</sup> came to different conclusions judging by routine MR imaging-detected abnormalities, revealing the association between clinical and imaging features. Therefore, conventional imaging examinations are insufficient to accurately assess brain damage in patients with GA-1.

On the basis of a Gaussian distribution model, DTI is used to quantitatively assess the damage to brain tissue. This approach can be widely applied to detect CNS metabolic disease changes, such as those of leukoencephalopathy with brainstem and spinal cord involvement and high lactate, metachromatic leukodystrophy, phenylketonuria, and Krabbe disease.<sup>11-14</sup> However, the displacement of water molecules is restricted by barriers, including cell membranes and organelles—that is, the movement of water molecules in the human body does not follow the Gaussian distribution. Hence, studies on biologic structures by DTI may be

inappropriate.<sup>15</sup> Diffusional kurtosis imaging (DKI) quantifies non-Gaussian diffusion of water in biologic systems and has been suggested to be advantageous over DTI; it better characterizes both normal and pathologic brain tissue and is particularly valuable for the assessment of GM.<sup>15</sup> The kurtosis reveals the degree of water diffusion restriction and brain tissue microstructural complexity.

To date, no studies have used DKI for the assessment of patients with GA-1. In this investigation, we used DKI to detect GM and WM microstructural changes in 17 patients with GA-1. We aimed to elucidate whether DKI parameters could be sufficiently sensitive to detect micropathologic changes in similar abnormal signal areas and whether they could be of value for severity evaluation.

## MATERIALS AND METHODS

### Subjects

This prospective study was performed in accordance with the Declaration of Helsinki for studies involving humans and after approval of the First Hospital of Jilin University internal review board (20K060-001) and the parents of the patients. The diagnosis of GA-1 was established by brain MR imaging and biochemical (urine organic acids and plasma acylcarnitines) and *GCDH* gene mutation analyses.<sup>16</sup> A group of 17 healthy controls (HCs) of similar age and sex were enrolled by community recruitment. All healthy subjects had no history of neurologic or psychiatric disorders and had normal MR imaging findings. The patients with GA-1 and HCs did not differ in either age or sex ( $P > .9$  in both instances) (Table). Written informed consent was obtained from parents or authorized legal representatives of all children who participated in the study. After diagnosis, metabolic

## Demographic characteristics of patients with GA-1 and healthy controls

Variable	GA-1 (n = 17)		HCs (n = 17)	
	Mean	Range	Mean	Range
Age (mo)	38 (SD, 17)	11–84	38 (SD, 17)	11–84
Sex (M/F)	6/11	–	6/11	–
BAD scores	14 (SD, 5)	4–22	0	0
Morbidity scores	2 (SD, 0.5)	1–3	0	0
Urinary glutaric acid ( $\mu\text{mol/mol}$ ) <sup>a</sup>	617 (SD, 725)	16.2–2937.62	–	–
Blood C5DC ( $\mu\text{mol/mol}$ )	4 (SD, 8)	0.19–38.07	–	–

**Note:**—C5DC indicates glutaryl carnitine; BAD, Barry-Albright dystonia; en dash, not applicable.

<sup>a</sup> Classified as high (urinary glutaric acid >100 mmol/mol) or low (<100 mmol/mol).

treatment was started in all patients with GA-1, including a lysine-free, low-lysine diet; a tryptophan-reduced amino acid formula; and other therapies for treating neurologic manifestations according to relevant guidelines.<sup>16</sup>

## MR Imaging

All patients were scanned using a 3T MR imaging system with a 32-channel head coil (Ingenia Elition X; Philips Healthcare). The sequences and parameters were as follows:

- 3D-T1WI: TR/TE = 6.6/3.0 ms, FOV = 240 × 240 × 170 mm, matrix = 240 × 240, in-plane resolution = 1 × 1 mm, section thickness = 1 mm, imaging time = 8 minutes 21 seconds.
- T2WI: TR/TE = 3600/1200 ms, FOV = 230 × 230 × 134 mm, matrix = 288 × 288, section thickness = 5 mm, imaging time = 1 minute 12 seconds.
- FLAIR: TR/TE = 9000/143 ms, FOV = 230 × 230 × 125 mm, matrix = 256 × 256, section thickness = 5 mm, imaging time = 2 minutes 42 seconds.
- DWI: single-shot echo-planar sequence. TR/TE = 2084/72 ms, FOV = 230 × 230 × 125 mm, matrix = 152 × 126, section thickness = 2.5 mm, imaging time = 0 minutes 25 seconds. A b-value of 1000 s/mm<sup>2</sup> was chosen.
- DKI: echo-planar imaging diffusion sequence with a total number of 55 diffusion-encoding directions. TR/TE = 4128/80 ms, FOV = 220 × 220 × 130 mm, matrix = 88 × 86, section thickness = 2.5 mm with a 1-mm gap, imaging time = 4 minutes 37 seconds. There were 3 b-values of 0, 1000, and 2000 s/mm<sup>2</sup>.

## Clinical and Neurologic Outcome and Neuroimaging Evaluation

Patients underwent a thorough history-taking, clinical examination, and neurologic-outcome assessment, management, and treatment. All patients with GA-1 and HCs were evaluated using the morbidity scores and Barry-Albright dystonia (BAD) scores.<sup>9,10,17</sup> Morbidity score items included loss of mobility, feeding problems, respiratory problems, and seizures necessitating treatment. A point was given for the presence of each item, with a total morbidity score ranging from 0 (asymptomatic) to 4 (severe morbidity). Dystonia severity was quantified using the BAD score, which is a 5-point, criterion-based, ordinal scale designed to assess dystonia in 8 body regions: eyes, mouth, neck, trunk, and the 4 extremities. Raters scored dystonia as none (0), slight (1), mild (2), moderate (3), and severe (4).

## Conventional MR Imaging Scores

In the study, MR imaging scores were analyzed on the basis of a previously described pattern-recognition approach of assessing GA-1.<sup>8-10</sup> All routine MR images of patients with GA-1 were independently reviewed and scored by authors B.B. and D.L., who have 10 and 21 years of experience with neuroimaging, respectively.

In addition, 2 reviewers were blinded to the clinical and biochemical examinations of patients. The cortex was scored as follows: 0 = unaffected, 1 = temporal atrophy, and 2 = frontotemporal atrophy. Each putamen, caudate, globus pallidus, thalamus, dentate, hippocampus, and cerebellum was rated as follows: 0 = unaffected, 1 = T2 hyperintensity, and 2 = atrophy. Each of the ventricles and external CSF spaces was rated as follows: 0 = unaffected, 1 = mildly/moderately dilated, and 2 = markedly dilated. Other scored abnormalities were of the WM (0 = unaffected, 1 = localized T2 hyperintensity, 2 = generalized/diffuse hyperintensity) and the subdural hematoma/hygroma (0 = none, 1 = unilateral, 2 = bilateral).

## DKI Analysis

DKI data of all patients were exported from the workstation and converted to the NIfTI data format by MRICron (<https://www.nitrc.org/projects/mricron/>). The NIfTI data were imported into the free software Diffusional Kurtosis Estimator (<http://www.nitrc.org/projects/dke>) for spatial smoothing, median filtering, linear trend removal, and denoise processing.<sup>18</sup>

Seven DKI metrics were extracted (Fig 2): mean kurtosis (MK), radial kurtosis (RK), axial kurtosis (AK), fractional anisotropy (FA), axial diffusivity (AD), radial diffusivity (RD), and mean diffusivity (MD). The metrics values were measured in the brain regions: bilateral dentate nucleus (DN), cerebellar hemisphere (CBH), pons (P), substantia nigra (SN), globus pallidus (GP), anterior putamen (AP), posterior putamen (PP), caudate head (CH), thalamus (Th), corona radiata (CR), centrum semiovale (CS), frontal lobes (FL), parietal lobes (PL), and temporal lobes (TL). The ROI (32 mm<sup>2</sup>: cerebellar hemisphere, pons, thalamus, and 16 mm<sup>2</sup>: other brain regions) method was applied in all subjects by a radiologist who had 10 years of experience in neuroimaging. All brain regions were measured 3 times bilaterally, and an average size was calculated to minimize the error value.

## Statistical Analysis

All statistical tests were performed using SPSS 22.0 statistical software (IBM). For DKI parameters in the ROIs, quantitative results are expressed as mean (SD). All data were tested for normality and variance homogeneity before analyses. A comparison between the patients with GA-1 and the control group of the same brain region was performed by *t* test for 2 independent samples to evaluate the

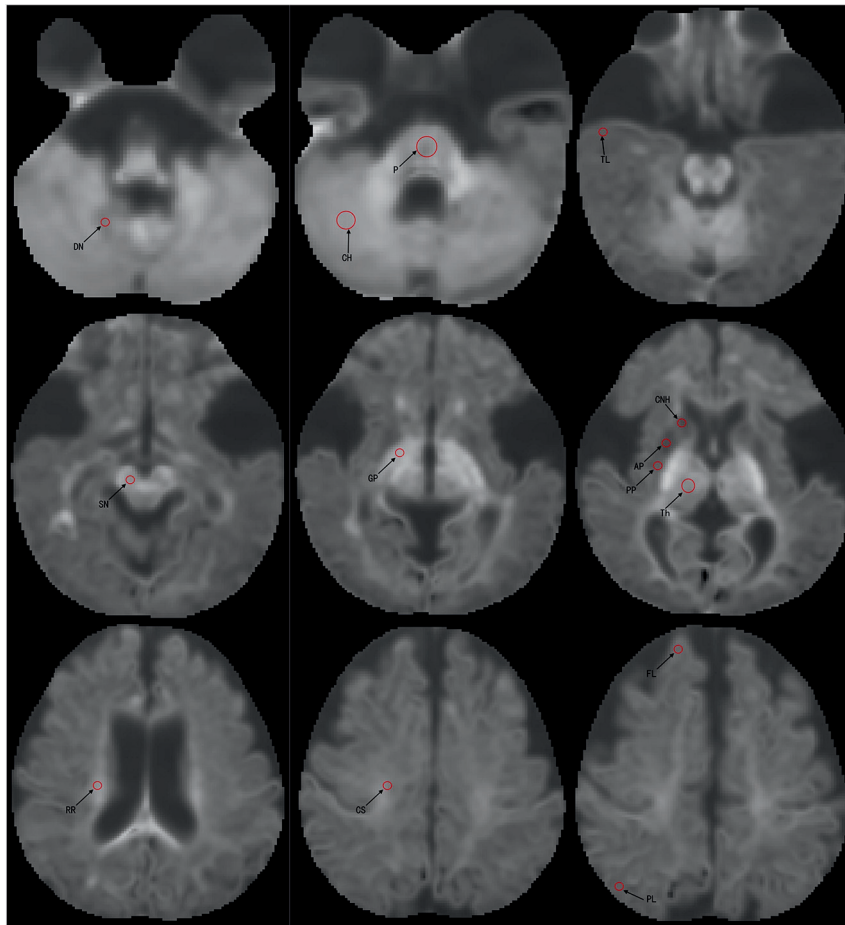


**FIG 2.** Example of the selection of ROIs (red circle) from the DN, CBH, P, SN, GP, AP, PP, CH, Th, CR, CS, FL, PL, and TL of patients with GA-1. Radiologists manually drew the ROIs (16 mm<sup>2</sup> and 32 mm<sup>2</sup>) on the gray level of the MK map.

DKI parameters. A  $P$  value  $< .05$  was considered to indicate a statistically significant difference. Qualitative data were expressed as frequency and percentage. A dichotomized design was applied for routine MR imaging findings, with interobserver reliability expressed as a Fleiss  $\kappa$ . The correlations between MR imaging and morbidity scores or BAD scores were tested statistically using the Mann-Whitney  $U$  statistic or the Kruskal-Wallis test.<sup>9,10</sup> The Pearson or Spearman correlation analysis was used to test the relationships between DKI parameters and morbidity scores or BAD scores. Receiver operating characteristic curve (ROC) analysis was used to evaluate the diagnostic performance of different brain region parameters with the strongest correlations. An area under the curve (AUC) of  $>0.5$  indicated a significant diagnostic value, and an AUC value closer to 1 was indicative of a better diagnostic value.

## RESULTS

### Study Population

We included 17 patients (11 female, 6 male) with confirmed GA-1 and complete information, including MR imaging findings and neurologic outcomes. A summary of demographic, clinical, and laboratory features, and MR imaging scores of patients with GA-1 is presented in the Online Supplemental Data. The mean age at MR imaging was 38.4 (SD, 17) months; median, 35 months; range,

11–84 months for all patients. Four (23.5%) patients with GA-1 had insidious onset, and 9 (52.9%) manifested acute onset, whereas 4 (23.5%) were asymptomatic. All patients had hypokinesia and dystonia, and one (5.8%) had a seizure during the MR imaging.

### Conventional MR Imaging Abnormalities and Association of MR Imaging Scores with the Morbidity and Barry-Albright Dystonia Scores

The MR imaging abnormalities of 17 patients with GA-1 are given in the Online Supplemental Data. 100% of the patients with GA-1 had expansion of the CSF anterior to the temporal lobes and widening of the Sylvian fissures, though the degrees of expansion were not always symmetric. Ventricle dilation was present in 94% of the examined patients ( $n = 16$ ). None of the patients had subdural hematoma/hygroma. WM changes were present in 88% of the patients ( $n = 15$ ). In the GM, the striatum had a high signal or atrophy on T2WI. The most frequently occurring abnormalities (100%) were of the putamen and the globus pallidus. The abnormalities of the caudate head, thalamus, dentate, hippocampus, and cerebellum were 59%, 18%, 47%, 23%, and 0, respectively. Six patients (35%) had hyperintensities in the corpus callosum. The central tegmental tract had restricted diffusion and low ADC in 4 patients (23%). The values of the



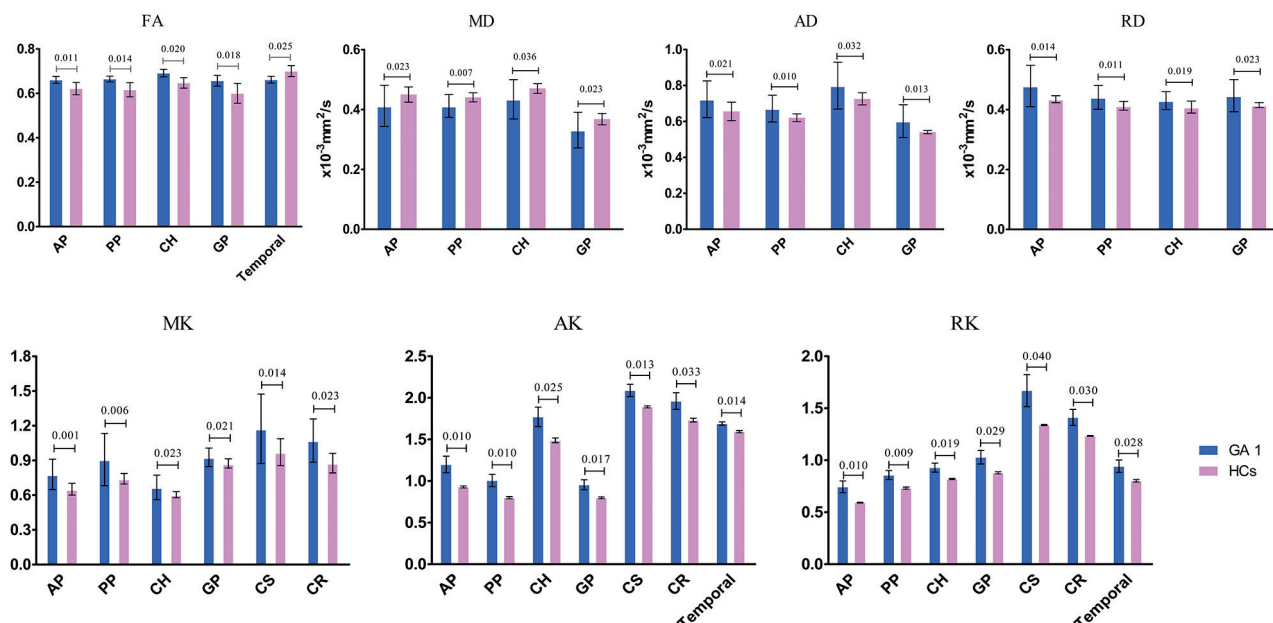


**FIG 3.** DKI values of ROI bar graphs in predefined ROIs with differences ( $P < .05$ ) in the patients with GA-1 and healthy groups.

associations of the MR imaging scores with the morbidity and BAD scores are given in the Online Supplemental Data. All brain regions showed no relation to the morbidity and BAD scores.

### Comparison of the Brain Region DKI Metrics in Patients with GA-1 and Healthy Subjects

The kurtosis metrics (MK, AK, and RK values) and FA, AD, and RD values of the AP, PP, CH, and GP of the GA-1 group were significantly higher than those of the corresponding brain region in the control group ( $P < .05$ ). The MD values of the AP, PP, CH, and GP in the GA-1 group were significantly lower than those in the control group ( $P < .05$ ). The MK, AK, and RK values of the CS and the CR in the GA-1 group were significantly higher than those in the control group ( $P < .05$ ). The RD, AD, AK, and RK values of the TL in the GA-1 group were higher, whereas the FA values were lower than those in the control group ( $P < .05$ ) (Fig 3). No significant difference was observed in the DKI parameters of other ROI between the 2 groups.

### Correlation between DKI Metrics and BAD Scores and Morbidity Scores

The data of the association of the DKI parameters of different ROIs with the BAD scores and morbidity scores are provided in the Online Supplemental Data. The results (Fig 4) show a negative correlation in the FA of the TL, MK, AK, and RK of the AP and PP; MK and AK of the GP; and MK of the CH, with significant differences (all,  $P < .05$ ). In addition, there was a significant positive association of the AD values of the TL ( $r = 0.596$ ,  $P = .012$ ) and the MD values of the PP ( $r = 0.548$ ,  $P = .023$ ) with the BAD scores.

### ROC Analyses for Diagnostic Performances

The values of MK in the AP, PP, CH and GP, as well as RK in the AP distinguished the patients with GA-1 ( $\text{AUC} > 0.5$ ,  $P < .05$ ),

among which the MK of the AP had the highest AUC (0.837), whereas the MK of the GP had the lowest AUC (0.723) (Fig 5).

## DISCUSSION

In patients with GA-1, acute striatal necrosis during infancy is the principal cause of morbidity and mortality, which leads to chronic oromotor, skeletal, and respiratory complications of dystonia.<sup>5</sup> A previous study revealed that routine MR imaging abnormalities may regress, be stable for years, or progress.<sup>8</sup> In our investigation, 17 patients with GA-1 manifested characteristic and region-specific brain MR imaging abnormalities (Online Supplemental Data), but no brain structure abnormality appeared to correlate with the morbidity and BAD scores (Table, all  $P > .05$ ), a finding inconsistent with the results of a previous study in which striatal necrosis was identified by routine MR imaging as the most reliable predictor of a movement disorder,<sup>8</sup> which may be related to the small sample size used in our research. In addition, Strauss et al found that older GA-1 patients with significant T2 or FLAIR hypersignal and intact basal ganglia could have normal motor function and neurocognitive performance, which also indicates that conventional MR has disadvantages in precisely assessing GA-1 patients' motor impairment.<sup>19</sup>

To better understand the mechanisms of gray/white matter damage, we first prospectively investigated the changes of the DKI parameters in 17 patients with GA-1. In many CNS diseases,<sup>20-22</sup> such as multiple sclerosis and Parkinson disease, DKI metrics have become an important biomarker for the detection of anisotropic and isotropic diffusion.<sup>23</sup> DKI provides not only the diffusion tensor metrics (FA, MD, AD, and RD) but also the kurtosis metrics (AK, RK, and MK).<sup>15,23</sup> Furthermore, kurtosis reveals the degree of diffusion restriction and tissue microstructural complexity. A change in the MK value depends on the structural complexity of the ROIs, and an increase of the MK value is due to increased cell-packing density and microstructural complexity.<sup>18,22</sup> AK and RK are of value for providing additional

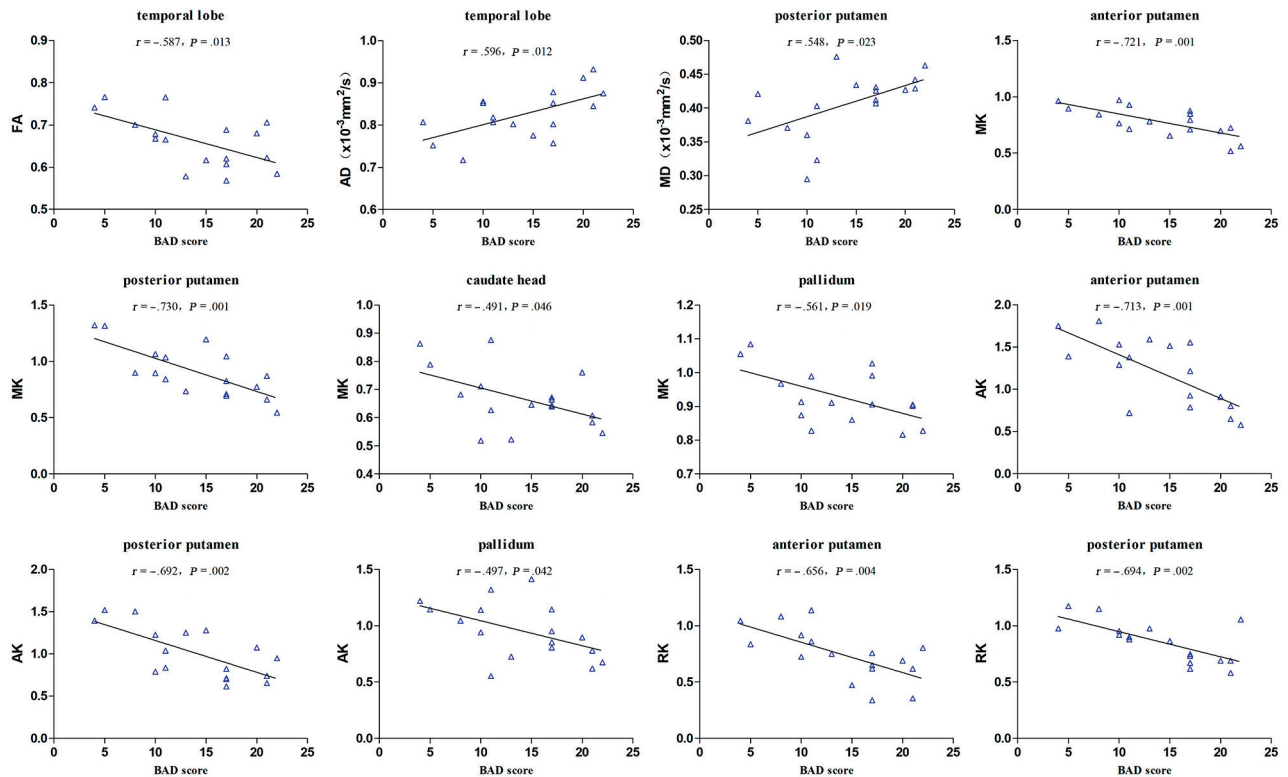


**FIG 4.** The association analyses with maximal correlation coefficients between the DKI metrics (FA, MD, MK, AK, and RK values) and the BAD scores.

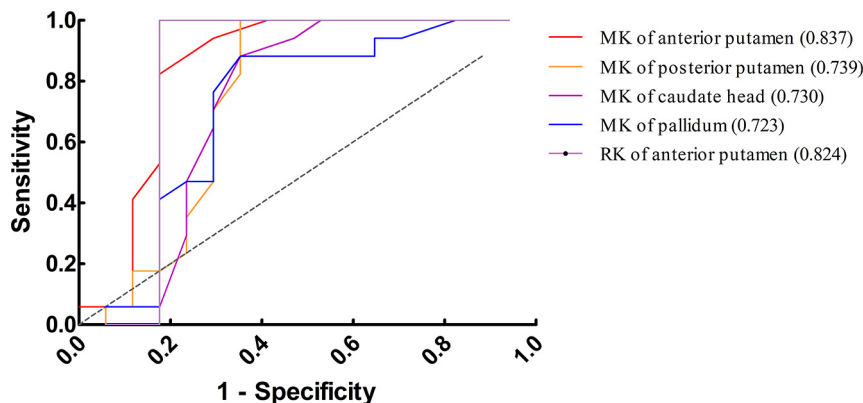


**FIG 5.** ROC curve analyses (AP, PP, CH and GP) were performed for the diagnosis of GA-1 to assess the diagnostic performance in the brain structures of the DKI parameters with the strongest correlation. The AUCs of different parameters were compared.

information of the axonal and myelin integrity of the WM bundles. The decrease in RK is associated with demyelination, whereas a change in AK reflects axonal degeneration. Additionally, increases in RD and AD are linked to myelin degeneration and axonal degeneration, respectively.<sup>24</sup>

GA-1 animal model studies show that the pathologic mechanism of brain injury is realized via cytotoxic edema, bilateral striatal neurodegeneration, neuronal swelling, and vacuole formation leading to cerebral capillary occlusion.<sup>5,25</sup> Thus, the extracellular tortuosity, decreased membrane permeability, and cell swelling during cytotoxic edema in specific brain regions of patients with GA-1 are

reflected by an increase in kurtosis metrics and FA. We found that the increase in MK, AK, and RK of the putamen, caudate head, and pallidum (Fig 3) could be related to cell swelling, ischemic state, and an increase in the volume fraction of limited water diffusion. The cytotoxic edema reduced the extracellular volume and restriction in water motion, which gave rise to a decrease in the MD value. In addition, the changes in MK, AK, and RK of the centrum semiovale and corona radiata revealed that water diffusion may be limited in the fiber structure and may be affected by the cytotoxic effect of glutaric acid, which may indicate that in patients with GA-1, kurtosis metrics are more sensitive to the damage of the WM

bundles than DTI metrics (FA, MD, AD, and RD). The kurtosis value is able to reflect the changes in microstructure in both WM and GM.<sup>26</sup> Temporal lobe atrophy is a common MR imaging manifestation, but the mechanism of its neuron damage is not fully understood.<sup>7</sup> In this study, RD, AD, AK, and RK of the temporal lobe were higher than those in the control group, indicating that the changes might be associated with the alterations of the glutaric acid level.

In our study, the significant correlation between the BAD score and DKI metrics, including the MK, AK, and RK in the putamen, caudate head, and pallidum, supported the hypothesis that striatum microstructural changes may contribute to a permanent motor

decline and dystonia (Fig 4). The anterior putamen MK values had the strongest correlations with the BAD scores compared with the FA, MD, AD, AK, and RK values. Thus, kurtosis metrics can serve as a sensitive imaging biomarker in detecting striatum pathology in patients with GA-1. Our results indicate that DKI enables the timely detection of changes in the brain tissue microstructure of patients with GA-1, which is more beneficial for the assessment of the disease severity compared with routine brain MR imaging scores. By comparing the diagnostic efficiency of DKI parameters, we found that the MK and RK of the anterior putamen (AUC = 0.837 and 0.824, respectively) in patients with GA-1 had a higher sensitivity for dystonia assessment than other parameters.

Our study has some limitations. First, the small sample size may have influenced the results. Second, the DKI metrics were measured on the basis of ROIs manually placed in various regions, which might have yielded imperfect reference values and thus bias. In addition, the ROI-based approach was focused on a limited number of spatially-defined regions within the brain, such as in the large WM tracts (eg, the corpus callosum). Third, more time points and longer time spans are required to better investigate the changes of the gray/white matter across time. Fourth, this was not a multicenter study; thus, its results may not be generalizable.

## CONCLUSIONS

To our knowledge, this is the first DKI study of GA-1. Using DKI, we compared the magnitude and direction of diffusion in patients with GA-1 with abnormalities in different brain areas to gain insight into the microstructure of the affected brain tissue. The kurtosis values could serve as a surrogate biomarker for assessment of putaminal damage and reflect dyskinesia, which is correlated with prognosis. In the future, longitudinal studies with larger samples and a greater age span are needed to understand the MR imaging markers of GA-1.

**Disclosure forms** provided by the authors are available with the full text and PDF of this article at [www.ajnr.org](http://www.ajnr.org).

## REFERENCES

- Hedlund GL, Longo N, Pasquali M. **Glutaric acidemia type 1.** *Am J Med Genet C Semin Med Genet* 2006;142C:86–94 [CrossRef Medline](#)
- Fu Z, Wang M, Paschke R, et al. **Crystal structures of human glutaryl-CoA dehydrogenase with and without an alternate substrate: structural bases of dehydrogenation and decarboxylation reactions.** *Biochemistry* 2004;43:9674–84 [CrossRef Medline](#)
- Schmiesing J, Lohmoller B, Schweizer M, et al. **Disease-causing mutations affecting surface residues of mitochondrial glutaryl-CoA dehydrogenase impair stability, heteromeric complex formation and mitochondria architecture.** *Hum Mol Genet* 2017;26:538–51 [CrossRef Medline](#)
- Funk CB, Prasad AN, Frosk P, et al. **Neuropathological, biochemical and molecular findings in a glutaric acidemia type 1 cohort.** *Brain* 2005;128:711–22 [CrossRef Medline](#)
- Zinnanti WJ, Lazovic J, Housman C, et al. **Mechanism of metabolic stroke and spontaneous cerebral hemorrhage in glutaric aciduria type I.** *Acta Neuropathol Commun* 2014;2:13 [CrossRef Medline](#)
- Boy N, Garbade SF, Heringer J, et al. **Patterns, evolution, and severity of striatal injury in insidious- vs acute-onset glutaric aciduria type 1.** *J Inherit Metab Dis* 2019;42:117–27 [CrossRef Medline](#)
- Ntorkou AA, Daire J, Renaldo F, et al. **Enlargement of the optic chiasm: a novel imaging finding in glutaric aciduria type I.** *AJNR Am J Neuroradiol* 2021;42:1722–26 [CrossRef Medline](#)
- Mohammad SA, Abdelkhalek HS, Ahmed KA, et al. **Glutaric aciduria type 1: neuroimaging features with clinical correlation.** *Pediatr Radiol* 2015;45:1696–705 [CrossRef Medline](#)
- Sadek AA, Aladawy MA, Magdy RM, et al. **Clinico-radiological correlation in 26 Egyptian children with glutaric acidemia type 1.** *Neuropediatrics* 2021;52:431–40 [CrossRef Medline](#)
- Garbade SF, Greenberg CR, Demirkol M, et al. **Unravelling the complex MRI pattern in glutaric aciduria type I using statistical models—a cohort study in 180 patients.** *J Inherit Metab Dis* 2014;37:763–73 [CrossRef Medline](#)
- Steenweg ME, Pouwels PJ, Wolf NI, et al. **Leucoencephalopathy with brainstem and spinal cord involvement and high lactate: quantitative magnetic resonance imaging.** *Brain* 2011;134:3333–41 [CrossRef Medline](#)
- van Rappard DF, Konigs M, Steenweg ME, et al. **Diffusion tensor imaging in metachromatic leukodystrophy.** *J Neurol* 2018;265:659–68 [CrossRef Medline](#)
- Clocksins HE, Hawks ZW, White DA, et al. **Inter- and intra-tract analysis of white matter abnormalities in individuals with early-treated phenylketonuria (PKU).** *Mol Genet Metab* 2021;132:11–18 [CrossRef Medline](#)
- Guo AC, Petrella JR, Kurtzberg J, et al. **Evaluation of white matter anisotropy in Krabbe disease with diffusion tensor MR imaging: initial experience.** *Radiology* 2001;218:809–15 [CrossRef Medline](#)
- Jensen JH, Helpert JA. **MRI quantification of non-Gaussian water diffusion by kurtosis analysis.** *NMR Biomed* 2010;23:698–710 [CrossRef Medline](#)
- Boy N, Muhlhausen C, Maier EM, et al. **Additional individual contributors. Proposed recommendations for diagnosing and managing individuals with glutaric aciduria type I: second revision.** *J Inherit Metab Dis* 2017;40:75–101 [CrossRef Medline](#)
- Barry MJ, VanSwearingen JM, Albright AL. **Reliability and responsiveness of the Barry-Albright Dystonia Scale.** *Dev Med Child Neurol* 1999;41:404–11 [CrossRef Medline](#)
- Qiao PG, Cheng X, Li GJ, et al. **MR diffusional kurtosis imaging-based assessment of brain microstructural changes in patients with Moyamoya disease before and after revascularization.** *AJNR Am J Neuroradiol* 2020;41:246–54 [CrossRef Medline](#)
- Strauss KA, Lazovic J, Wintermark M, et al. **Multimodal imaging of striatal degeneration in Amish patients with glutaryl-CoA dehydrogenase deficiency.** *Brain* 2007;130:1905–20 [CrossRef Medline](#)
- Guglielmetti C, Veraart J, Roelant E, et al. **Diffusion kurtosis imaging probes cortical alterations and white matter pathology following cuprizone induced demyelination and spontaneous remyelination.** *Neuroimage* 2016;125:363–77 [CrossRef Medline](#)
- Tan S, Hartono S, Welton T, et al. **Utility of quantitative susceptibility mapping and diffusion kurtosis imaging in the diagnosis of early Parkinson's disease.** *Neuroimage Clin* 2021;32:102831 [CrossRef Medline](#)
- Spampinato MV, Chan C, Jensen JH, et al. **Diffusional kurtosis imaging and motor outcome in acute ischemic stroke.** *AJNR Am J Neuroradiol* 2017;38:1328–34 [CrossRef Medline](#)
- Marralle M, Collura G, Brai M, et al. **Physics, techniques and review of neuroradiological applications of diffusion kurtosis imaging (DKI).** *Clin Neuroradiol* 2016;26:391–403 [CrossRef Medline](#)
- Helpert JA, Adisetiyo V, Falangola MF, et al. **Preliminary evidence of altered gray and white matter microstructural development in the frontal lobe of adolescents with attention-deficit hyperactivity disorder: a diffusional kurtosis imaging study.** *J Magn Reson Imaging* 2011;33:17–23 [CrossRef Medline](#)
- Isasi E, Korte N, Abudara V, et al. **Glutaric acid affects pericyte contractility and migration: possible implications for GA-I pathogenesis.** *Mol Neurobiol* 2019;56:7694–707 [CrossRef Medline](#)
- Hori M, Fukunaga I, Masutani Y, et al. **Visualizing non-Gaussian diffusion: clinical application of q-space imaging and diffusional kurtosis imaging of the brain and spine.** *Magn Reson Med Sci* 2012;11:221–33 [CrossRef Medline](#)